J. Phase Equilib. Diffus. (2019) 40:176–187
https://doi.org/10.1007/s11669-019-00712-4

Phase Equilibria in the Al-Sn-Co Ternary System

X. J. Liu[1,2] · H. W. Zou[1] · J. B. Zhang[1] · S. Y. Yang[1] · Y. Lu[1] · J. J. Han[1] · J. H. Zhu[1] · X. R. Chen[1] · C. P. Wang[1]

Submitted: 20 August 2018 / in revised form: 24 December 2018 / Published online: 20 February 2019

Abstract The isothermal sections of the Al-Sn-Co ternary system at 800 °C and 1000 °C were constructed by twenty-nine key samples and two solid–liquid diffusion couples using electron probe microanalysis and x-ray diffraction analysis. The results show that: (1) No ternary intermetallic compound was found in this ternary system at 800 °C and 1000 °C. (2) The solid solubility of Sn in the Al-Co binary compounds is very small. (3) As-cast $Al_{47}Sn_{47}Co_6$, $Al_{46}Sn_{46}Co_8$ and $Al_{45}Sn_{45}Co_{10}$ (at.%) alloys exhibit the separated macroscopic morphologies. The reason is that the addition of Co can significantly promote the metastable liquid-phase separation in Al-Sn binary system. The newly determined phase equilibria may contribute to thermodynamic assessment and development of Al-based alloys.

Keywords Al-Sn-Co · phase diagram · phase equilibria · liquid miscibility gap

1 Introduction

Aluminum-water reaction is a cheap, effective, environment-friendly and safe method of preparing hydrogen.[1–3] Al-based alloys milled with low-melting-point metals[4–6] and other active metals[7–9] have good hydrogen production properties. Recently, using self-assembling egg-type powders with core/shell microstructure induced by liquid miscibility gap,[10] Wang et al. reported that a kind of self-assembling powder has better activity to generate H_2.[11] Al-Sn binary system has metastable liquid miscibility gap over a wide composition range, which is a good candidate for further optimizing of self-assembling powders.[12]

In practical application, the aim of adding the third element is to control the formation of some special macroscopic and microscopic morphologies of powders, because the third element can enhance or reduce the extent of liquid phase separation.[13,14] For example, in Al-Bi-Sn ternary system, Bi additions to the Al-Sn binary system can significantly promote the metastable liquid miscibility gap.[15] It is possible that the Co, Cu, Fe, Ni and other element additions may have an influence on liquid phase separation in Al-Sn binary system. In addition, according to the literature,[16] the addition of Co can significantly improve the production of hydrogen in Al-H_2O reaction. Thus it is of great importance to obtain a clear understanding of the Al-Sn-Co ternary phase equilibria.

Three corresponding binary systems Al-Sn,[15,17–21] Al-Co[22–25] and Co-Sn[26–28] have been well investigated. Liu et al.[15] reported experimental investigation and thermodynamic calculation in Al-Bi-Sn ternary system. And there is metastable liquid miscibility gap in Al-Sn binary system. Stein et al.[23] updated thermodynamic description of Al-Co system which exhibits five stable compounds (AlCo, Al_5Co_2, Al_3Co, $Al_{13}Co_4$ and Al_9Co_2). Liu et al.[26] made thermodynamic assessment of Co-Sn binary system, where there are three stable compounds (Co_3Sn_2, CoSn and $CoSn_2$). Three binary phase diagrams of Al-Sn, Al-Co and Co-Sn constituting the Al-Sn-Co ternary system are shown in Fig. 1. Information on the stable solid phases and crystal

✉ C. P. Wang
wangcp@xmu.edu.cn

1 College of Materials and Fujian Provincial Key Laboratory of Materials Genome, Xiamen University, Xiamen 361005, People's Republic of China

2 State Key Laboratory of Advanced Welding and Joining, Harbin Institute of Technology, Shenzhen 518005, People's Republic of China

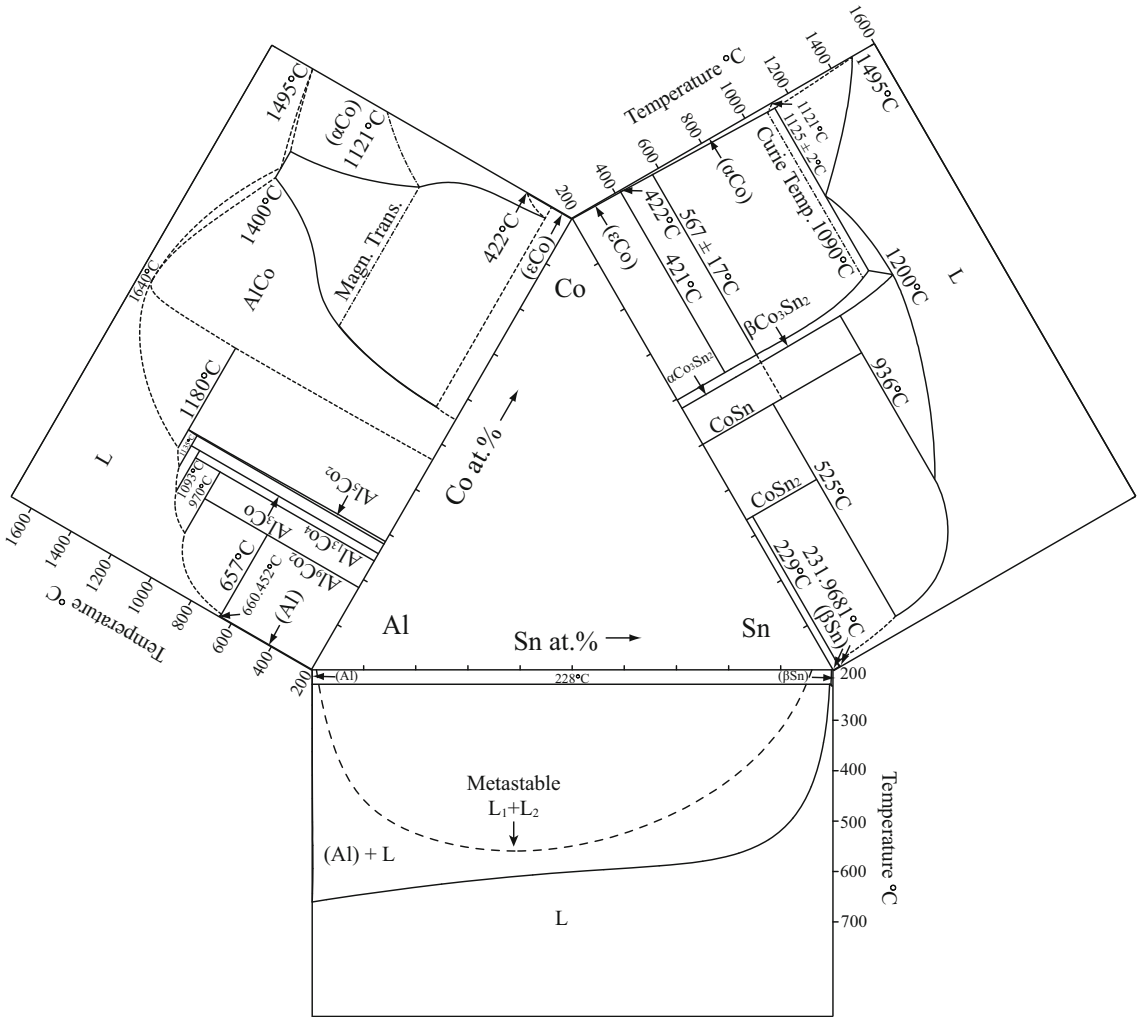

Fig. 1 Binary phase diagrams constituting the Al-Sn-Co ternary system[16,23,26]

Table 1 Stable solid phases in the three binary systems[21,25,28]

System	Phase	Phase symbol	Prototype	Strukturbericht	Space group	References
Al-Sn	(Al)	*cF*4	Cu	A1	*Fm-3 m*	20
	(βSn)	*tI*4	βSn	A5	$I4_1/amd$	20
Al-Co	(αCo)	*cF*4	Cu	A1	*Fm-3 m*	24
	(εCo)	*hP*2	Mg	A3	$P6_3/mmc$	24
	AlCo	*cP*2	CsCl	B_2	*Pm-3 m*	24
	Al_5Co_2	*hP*28	Al_5Co_2	$D8_{11}$	$P6_3/mmc$	24
	Al_3Co	…	…	…	…	24
	$Al_{13}Co_4$	*oP*102	$Al_{13}Co_4$	…	$Pmn2_1$	24
	Al_9Co_2	*mP*22	Al_9Co_2	…	$P2_1/a$	24
Co-Sn	(αCo)	*cF*4	Cu	A1	*Fm-3 m*	27
	(εCo)	*hP*2	Mg	A3	$P6_3/mmc$	27
	(βSn)	*tI*4	βSn	A5	$I4_1/amd$	27
	αCo_3Sn_2	*oP*20	Ni_3Sn_2	…	*Pnma*	27
	βCo_3Sn_2	*hP*6	Ni_2In	$B8_2$	$P6_3/mmc$	27
	CoSn	*hP*6	CoSn	…	*P6/mmm*	27
	$CoSn_2$	*tI*12	$CuAl_2$	C16	*I4/mcm*	27

structures in three binary systems are summarized in Table 1.[21,25,28] However, there is no information about Al-Sn-Co ternary system in the relevant literature.

The purpose of this work is to experimentally investigate phase equilibria in the Al-Sn-Co ternary system at 800 and 1000 °C. The results acquired in the present work are expected to contribute to the available thermodynamic and phase diagram information to enable more extensive application of this system.

2 Experimental Procedures

In order to obtain phase relations, twenty-nine key samples together with two solid–liquid diffusion couples were prepared. The diffusion couple is a powerful and efficient technique for mapping the phase diagrams of ternary systems.[29–31] Within diffusion layers the equilibrium phases occur, whereas local equilibria take place at the interface. However, it is possible that phases may be missed by the

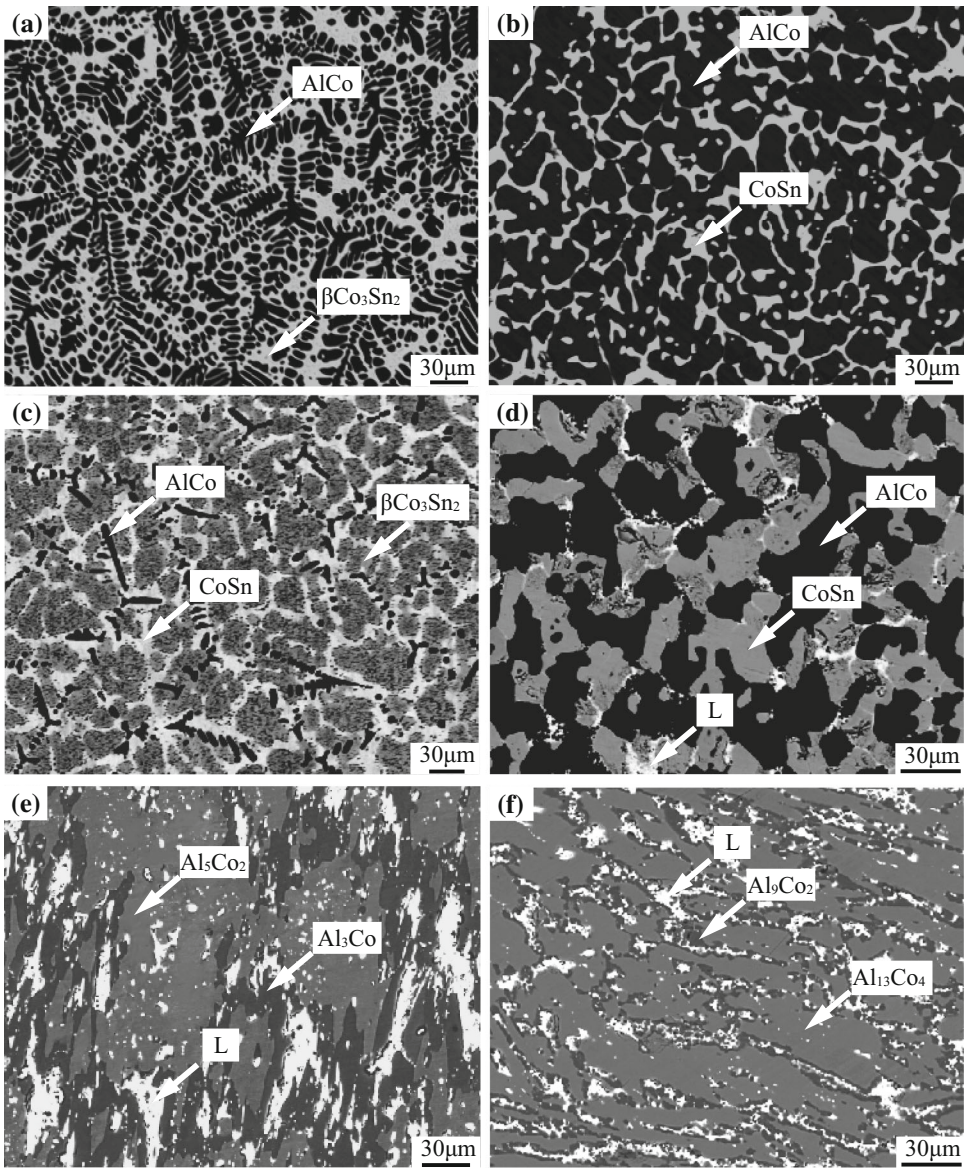

Fig. 2 Typical ternary BSE images obtained from: (a) $Al_{34}Sn_{10}Co_{56}$ alloy annealed at 800 °C for 30 days; (b) $Al_{40}Sn_6Co_{54}$ alloy annealed at 800 °C for 30 days; (c) $Al_8Sn_{40}Co_{52}$ alloy annealed at 800 °C for 30 days; (d) $Al_{25}Sn_{30}Co_{45}$ alloy annealed at 800 °C for 4 days; (e) $Al_{71}Sn_4Co_{25}$ alloy annealed at 800 °C for 4 days; (f) $Al_{76}Sn_4Co_{20}$ alloy annealed at 800 °C for 4 days

diffusion couple for determining the phase diagram.[31,32] Because slow nucleation of the phase can prevents formation of the diffusion layer. In order to obtain more reliable information, Kodentsov et al.,[31] among others, suggested combining key sample analysis with the diffusion couple method. Therefore, two technologies were used in the present work.

The buttons of the key samples were melted from 99.99 wt.% Al and 99.99 wt.% Sn and 99.99 wt.% Co in an argon arc furnace, using a nonconsumable tungsten electrode. In order to achieve homogeneity, the ingots were melted four times. After each melt, ingots were reversed to promote mixing. The sample weight was around 15 g and the weight loss during melting was generally $< 0.20\%$ of the sample weight. Then ingots of alloys were cut into small pieces which are about 2 g. After wrapped in tantalum foil, specimens were sealed into silica tubes under purified Ar gas. Specimens were annealed at 800 °C and 1000 °C for different time. The annealing time depends on the annealing temperature and the composition of specimens. Then specimens were quenched into ice water. Solid–liquid diffusion couples were prepared from two end-members of pure Co and $Al_{50}Sn_{50}$ (at.%) which were prepared in argon arc furnace. Then the button of Co was cut into cubes with a volume of $4 \times 4 \times 7$ mm^3. After standard metallographic preparation, Co and $Al_{50}Sn_{50}$ (at.%) were put into

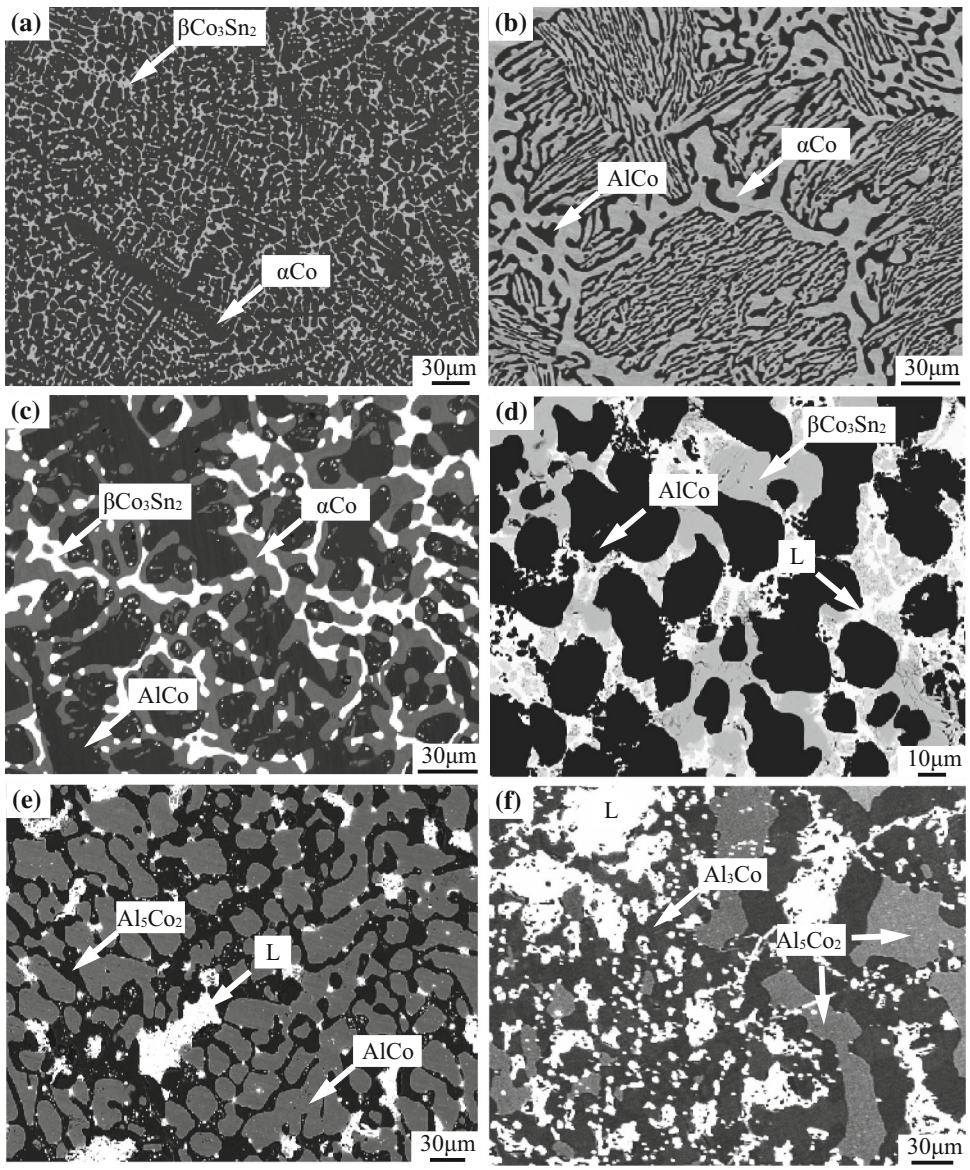

Fig. 3 Typical ternary BSE images obtained from: (a) $Al_3Sn_7Co_{90}$ alloy annealed at 1000 °C for 15 days; (b) $Al_{19}Sn_1Co_{80}$ alloy annealed at 1000 °C for 15 days; (c) $Al_{22}Sn_5Co_{73}$ alloy annealed at 1000 °C for 15 days; (d) $Al_{25}Sn_{30}Co_{45}$ alloy annealed at 1000 °C for 2 days; (e) $Al_{55}Sn_{11}Co_{34}$ alloy annealed at 1000 °C for 2 days; (f) $Al_{70}Sn_7Co_{23}$ alloy annealed at 1000 °C for 2 days

the alumina crucible. Crucibles wrapped in sealed silica tubes under purified Ar gas were annealed at 800 °C for 40 min and at 1000 °C for 20 min. After quenching in ice water, samples were cut from the middle for observation. Solid–liquid diffusion couples of $Co/Al_{50}Sn_{50}$ annealed at 800 °C for 40 min and $Co/Al_{50}Sn_{50}$ annealed at 1000 °C for 20 min are denoted as diffusion couple 1 and diffusion couple 2, respectively.

After standard metallographic preparation, the macrostructural observations were carried out by high resolution camera. The equilibrium compositions of the phases and microstructural observations were measured by electron probe microanalysis (EPMA) (JXA-8100R, JEOL, Japan). Pure elements were used as standards and the measurements were carried out at 20.0 kV and 1.0×10^{-8} mA. Energy Dispersive Spectrometer (EDS) was used to determine the compositions of the liquid phase. The liquid phase was measured by EDS analysis at least 10 times. Then the data was averaged. The x-ray diffraction (XRD) was used to identify the constituent phases. The XRD measurement was carried out on a Phillips Panalytical X-pert diffractometer using Cu K_α radiation at 40.0 kV and 40 mA. The data were collected in the range of 2θ from 10° to 90° at a step with of 0.0167°.

3 Results and Discussion

3.1 Microstructure

Figure 2 and 3 show the BSE (back-scattered electron) images of typical ternary Al-Sn-Co alloys. Phase identification depends on equilibrium compositions and XRD results. All the mentioned chemical compositions in this work were given in form of atomic ratio (at.%). The L in this work means liquid phase. In Fig. 2(a, b), there are two two-phase equilibria of AlCo + βCo_3Sn_2 and AlCo + CoSn that were found in alloys $Al_{34}Sn_{10}Co_{56}$ and $Al_{40}Sn_6Co_{54}$ annealed at 800 °C for 30 days. The EPMA results indicated that βCo_3Sn_2 and CoSn are matrices where AlCo is distributed in them. As illustrated in Fig. 2(c, d), two three-phase equilibria of AlCo (black) + βCo_3Sn_2 (dark gray) + CoSn (light gray) and AlCo (black) + CoSn (gray) + L (white) were detected in alloy $Al_8Sn_{40}Co_{52}$ annealed at 800 °C for 30 days and alloy $Al_{25}Sn_{30}Co_{45}$ annealed at 800 °C for 4 days, respectively. Figure 2(e) illustrates that three-phase equilibrium of Al_5Co_2 + Al_3Co + L existed in alloy $Al_{71}Sn_4Co_{25}$ annealed at 800 °C for 4 days, which was confirmed by the XRD result shown in Fig. 4(a). As can be seen from the Fig. 2(e), the black phase is Al_3Co, the gray one is Al_5Co_2 and the rest is liquid (*L*). All phases' diffraction peaks show good consistency and characteristic peaks of liquid phase originate from the Sn-rich phase. In addition, the microstructure of $Al_{13}Co_4$ + Al_9Co_2 + *L* in alloy $Al_{76}Sn_4Co_{20}$ annealed at 800 °C for 4 days is shown in Fig. 2(f) and substantiated by XRD result as shown in

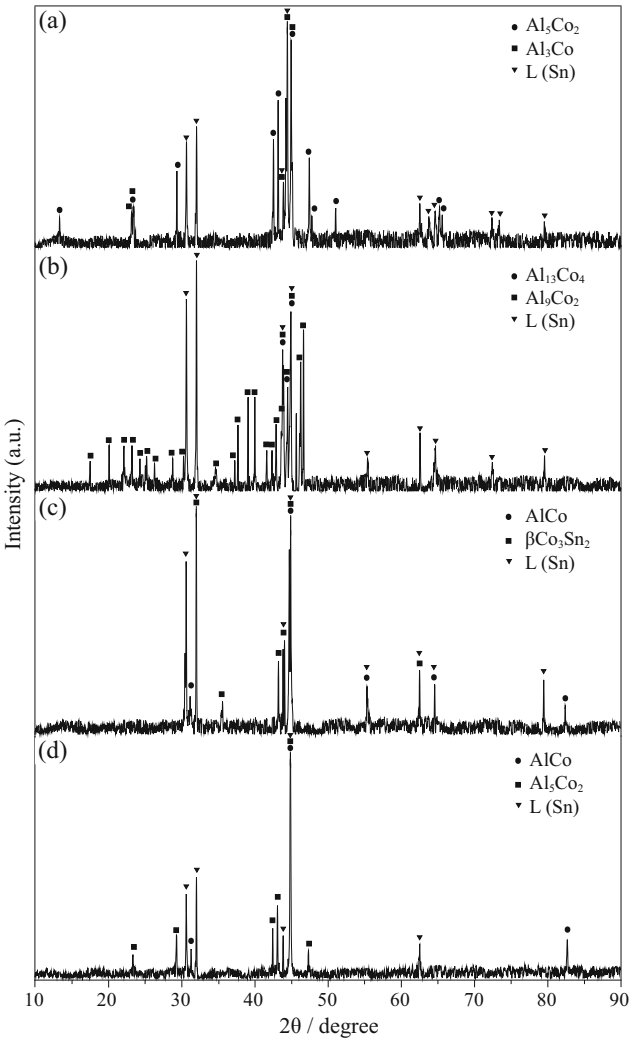

Fig. 4 X-ray diffraction patterns obtained from: (a) $Al_{71}Sn_4Co_{25}$ alloy annealed at 800 °C for 4 days; (b) $Al_{76}Sn_4Co_{20}$ alloy annealed at 800 °C for 4 days; (c) $Al_{25}Sn_{30}Co_{45}$ alloy annealed at 1000 °C for 2 days; (d) $Al_{55}Sn_{11}Co_{34}$ alloy annealed at 1000 °C for 2 days

Table 2 Equilibrium compositions of the Al-Sn-Co ternary system determined in the present work

T, °C	Alloy, at.%	Annealed time	Phase equilibria	Composition, at.%					
			Phase 1/Phase 2/Phase 3	Phase 1		Phase 2		Phase 3	
				Sn	Co	Sn	Co	Sn	Co
800	$Al_3Sn_7Co_{90}$	30 days	αCo/βCo_3Sn_2	1.6	94.8	37.9	61.1	…	…
	$Al_{19}Sn_1Co_{80}$	30 days	αCo/AlCo/βCo_3Sn_2	0.5	91.7	0.7	61.0	37.3	61.5
	$Al_{29}Sn_{12}Co_{59}$	30 days	AlCo/βCo_3Sn_2	0.8	57.5	38.8	60.0	…	…
	$Al_{34}Sn_{10}Co_{56}$	30 days	AlCo/βCo_3Sn_2	0.6	55.3	39.3	59.5	…	…
	$Al_8Sn_{40}Co_{52}$	30 days	AlCo/βCo_3Sn_2/CoSn	1.8	54.8	40.0	58.1	49.8	49.5
	$Al_{40}Sn_6Co_{54}$	30 days	AlCo/CoSn	0.6	54.0	49.4	49.1	…	…
	$Al_{25}Sn_{30}Co_{45}$	4 days	AlCo/CoSn/L	0.4	50.6	49.5	49.9	96.2	3.0
	$Al_{44}Sn_{14}Co_{42}$	4 days	AlCo/L	0.2	48.2	97.6	1.3	…	…
	$Al_{55}Sn_{11}Co_{34}$	4 days	AlCo/Al_5Co_2/L	0.3	46.9	0.1	27.4	96.0	1.1
	$Al_{71}Sn_4Co_{25}$	4 days	Al_5Co_2/Al_3Co/L	0.1	27.7	0.1	25.3	94.0	1.7
	$Al_{76}Sn_4Co_{20}$	4 days	$Al_{13}Co_4$/Al_9Co_2/L	0.1	23.9	0.2	18.3	93.1	1.6
	$Al_{48}Sn_{48}Co_4$	4 h	Al_9Co_2/L	0.1	17.8	56.6	0.4	…	…
	$Al_{81}Sn_5Co_{14}$	4 h	Al_9Co_2/L	0.1	17.2	20.7	0.5	…	…
	$Al_{87}Sn_2Co_{11}$	4 h	Al_9Co_2/L	0.1	17.6	5.1	0.4	…	…
	$Co/Al_{50}Sn_{50}$	40 min	AlCo/L	0.4	48.7	98.1	1.2	…	…
			Al_5Co_2/L	0.3	26.9	96.0	1.6	…	…
			Al_3Co/L	0.4	25.2	95.5	1.5	…	…
			$Al_{13}Co_4$/L	0.5	23.7	94.9	1.2	…	…
			Al_9Co_2/L	0.1	17.7	95.1	0.9	…	…
1000	$Al_3Sn_7Co_{90}$	15 days	αCo/βCo_3Sn_2	1.7	94.8	37.9	61.7	…	…
	$Al_6Sn_9Co_{85}$	15 days	αCo/βCo_3Sn_2	1.7	90.9	37.0	62.1	…	…
	$Al_{22}Sn_5Co_{73}$	15 days	αCo/AlCo/βCo_3Sn_2	1.4	86.7	1.4	66.5	34.3	62.8
1000	$Al_{19}Sn_1Co_{80}$	15 days	αCo/AlCo	1.1	86.9	0.8	65.5	…	…
	$Al_{15}Sn_{22}Co_{63}$	15 days	AlCo/βCo_3Sn_2	1.0	66.2	35.2	62.0	…	…
	$Al_{33}Sn_5Co_{62}$	15 days	AlCo/βCo_3Sn_2	0.7	62.4	35.9	61.0	…	…
	$Al_{29}Sn_{12}Co_{59}$	15 days	AlCo/βCo_3Sn_2	0.6	59.0	37.6	60.0	…	…
	$Al_{34}Sn_{10}Co_{56}$	15 days	AlCo/βCo_3Sn_2	0.8	55.1	37.9	59.5	…	…
	$Al_{25}Sn_{30}Co_{45}$	2 days	AlCo/βCo_3Sn_2/L	0.5	51.4	39.4	58.7	86.7	12.8
	$Al_{40}Sn_{21}Co_{39}$	2 days	AlCo/L	0.2	49.2	94.8	1.9	…	…
	$Al_{55}Sn_{11}Co_{34}$	2 days	AlCo/Al_5Co_2/L	0.1	46.7	0.1	27.6	94.9	1.2
	$Al_{70}Sn_7Co_{23}$	2 days	Al_5Co_2/Al_3Co/L	0.1	27.1	0.1	24.7	93.9	1.3
	$Al_{48}Sn_{48}Co_4$	2 h	$Al_{13}Co_4$/L	0.1	24.0	53.2	0.6	…	…
	$Al_{57}Sn_{40}Co_3$	2 h	$Al_{13}Co_4$/L	0.1	23.6	42.9	0.9	…	…
	$Al_{81}Sn_5Co_{14}$	2 h	$Al_{13}Co_4$/L	0.1	24.5	7.4	9.6	…	…
	$Co/Al_{50}Sn_{50}$	20 min	AlCo/L	0.3	49.4	90.7	8.8	…	…
			Al_5Co_2/L	0.5	27.3	95.1	1.3	…	…
			Al_3Co/L	0.4	25.2	94.3	1.2	…	…
			$Al_{13}Co_4$/L	0.4	23.4	94.0	1.0	…	…

Fig. 4(b). Two two-phase equilibria of αCo + βCo_3Sn_2 and αCo + AlCo were detected in alloys $Al_3Sn_7Co_{90}$ and $Al_{19}Sn_1Co_{80}$ in Fig. 3(a, b). As shown in Fig. 2(a), the βCo_3Sn_2 is gray matrix where the αCo (black) is uniformly distributed. In Fig. 3(c), there is a three-phase microstructure of αCo (gray) + AlCo (black) + βCo_3Sn_2

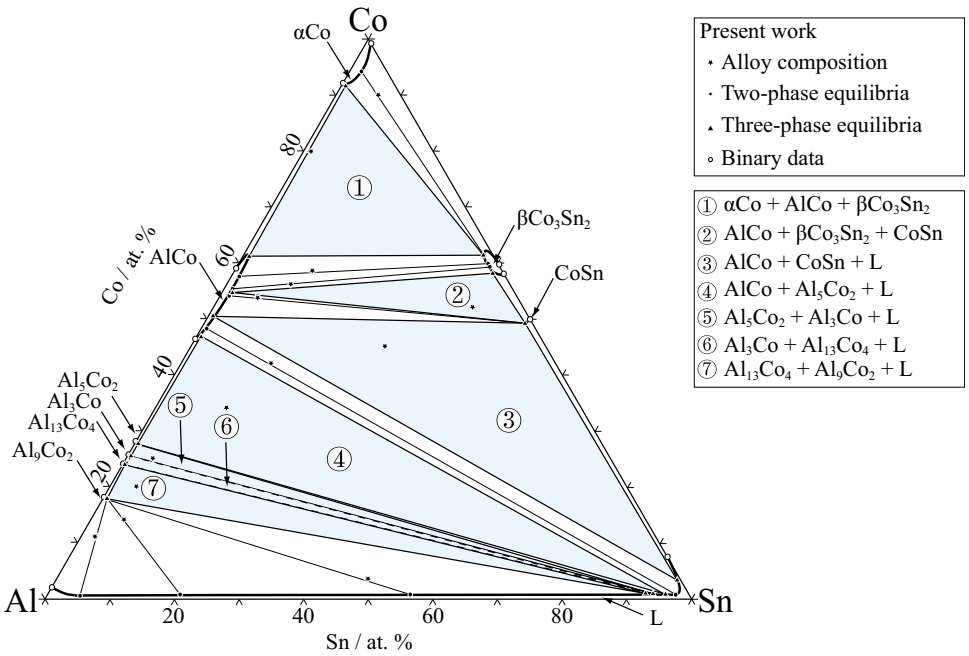

Fig. 5 Experimentally determined isothermal section of Al-Sn-Co system at 800 °C

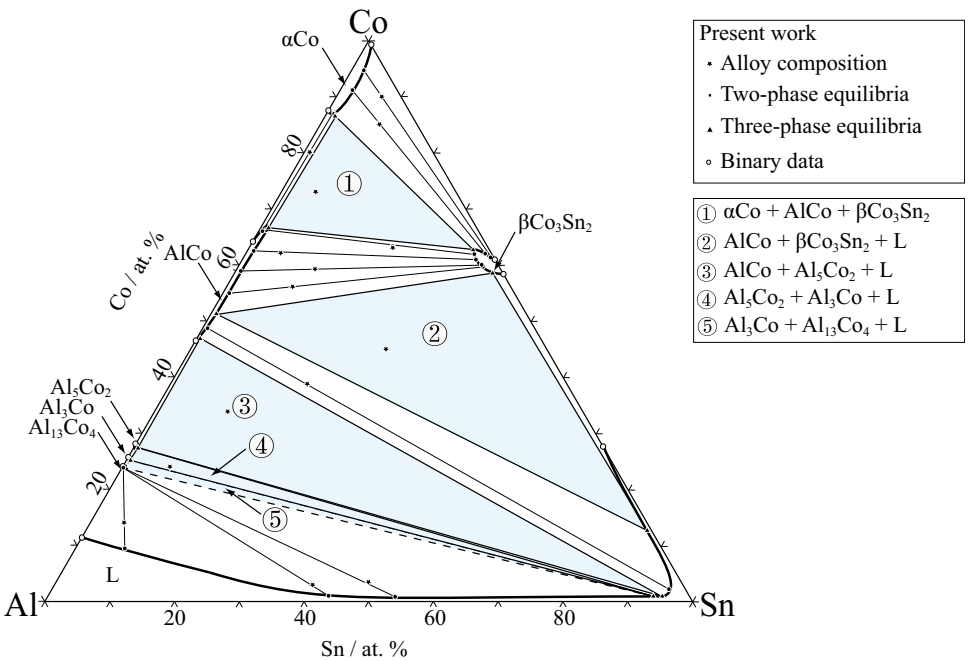

Fig. 6 Experimentally determined isothermal section of Al-Sn-Co system at 1000 °C

(white) in alloy $Al_{22}Sn_5Co_{73}$ that was annealed at 1000 °C for 15 days. Two three-phase microstructures of $AlCo + \beta Co_3Sn_2 + L$ and $AlCo + Al_5Co_2 + L$ were found in alloys $Al_{25}Sn_{30}Co_{45}$ and $Al_{55}Sn_{11}Co_{34}$ annealed at 1000 °C for 2 days, respectively (Fig. 3d, e). And the XRD results show very good consistency in Fig. 4(c, d). As similar to the previously discussed alloy $Al_{71}Sn_4Co_{25}$ annealed at 800 °C, these characteristic peaks of liquid

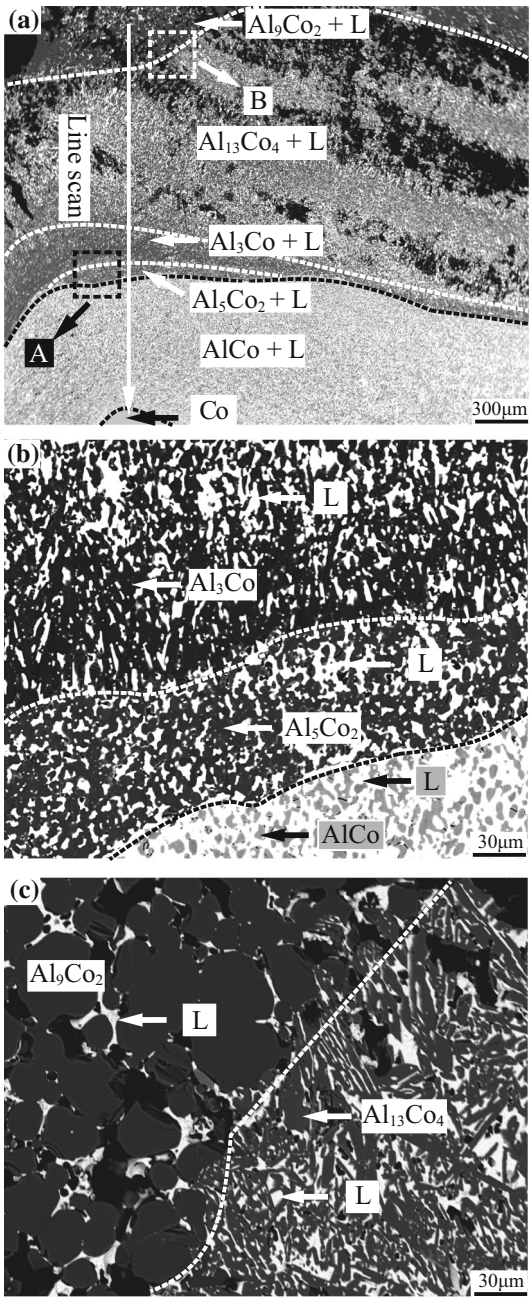

Fig. 7 (a) BSE images of diffusion couple 1; (b) Magnified area of "A" in (a); (c) Magnified area of "B" in (a)

phases also originate from the Sn-rich phase. As shown in Fig. 3(f), three-phase equilibrium of Al_5Co_2 (gray) + Al_3Co (black) + *L* (white) was discovered in the alloy $Al_{70}Sn_7Co_{23}$ annealed at 1000 °C for 2 days. Since the average atomic numbers of Al_5Co_2 and Al_3Co are approximate, their colors are also very similar.

3.2 Isothermal Section

Equilibrium compositions of the Al-Sn-Co ternary system in the present study at 800 °C and 1000 °C determined by EPMA are listed in Table 2. According to the experimental data, two isothermal sections at 800 °C and 1000 °C are shown in Fig. 5 and 6. Six three-phase regions of $\alpha Co + AlCo + \beta Co_3Sn_2$, $AlCo + \beta Co_3Sn_2 + CoSn$, $AlCo + CoSn + L$, $AlCo + Al_5Co_2 + L$, $Al_5Co_2 + Al_3Co + L$ and $Al_{13}Co_4 + Al_9Co_2 + L$ were experimentally determined at 800 °C. Four three-phase regions of $\alpha Co + AlCo + \beta Co_3Sn_2$, $AlCo + \beta Co_3Sn_2 + L$, $AlCo + Al_5Co_2 + L$ and $Al_5Co_2 + Al_3Co + L$ were also obtained at 1000 °C. It can be seen from Fig. 5 that there was small solid solubility of Sn in the Al-Co binary compounds at 800 °C. The solubility of Sn in αCo and AlCo phases was measured to be about 1.6 at.% and 1.8 at.%, respectively. The solubility of Sn in Al_5Co_2, Al_3Co, $Al_{13}Co_4$ and Al_9Co_2 was almost negligible. In addition, the solubility of Al in βCo_3Sn_2 and CoSn was measured to be about 1.9 at.% and 0.7 at.%, respectively. Compared the isothermal section at 1000 °C with that at 800 °C, the solubility of Sn in Al-Co binary compounds and the solubility of Al in Co-Sn binary compounds were also small. At 800 and 1000 °C, both isothermal sections have large liquid regions. With increasing temperature, the solubility of Co in liquid phase increases in Al-rich corner.

When the phase equilibrium was constructed in Al-rich corner at 800 °C, the three-phase region of $Al_3Co + Al_{13}Co_4 + L$ was not determined by key sample because of the small range. Besides this reason, compositions of as-cast alloys that are in the small three-phase region were in the region of phase separation. There is also a three-phase region of $Al_3Co + Al_{13}Co_4 + L$ that was not determined in the isothermal section at 1000 °C by key samples.

3.3 Solid–Liquid Diffusion Couples

Two diffusion couples were prepared. BSE images of diffusion couple 1 are shown in Fig. 7. During the heat treatment, extensive interdiffusion among Al, Sn and Co took place resulting in the formation of various equilibrium phases. It is very difficult to obtain a better diffusion layer due to the formation of cracks and uncontrolled diffusion time during the heat treatment. Usually, the use of diffusion couples in phase diagram studies is based on the assumption of local equilibrium at the phase interfaces. The solid–liquid diffusion is more complex because the diffusion of liquid phase is very quick thus it is difficult to find out the

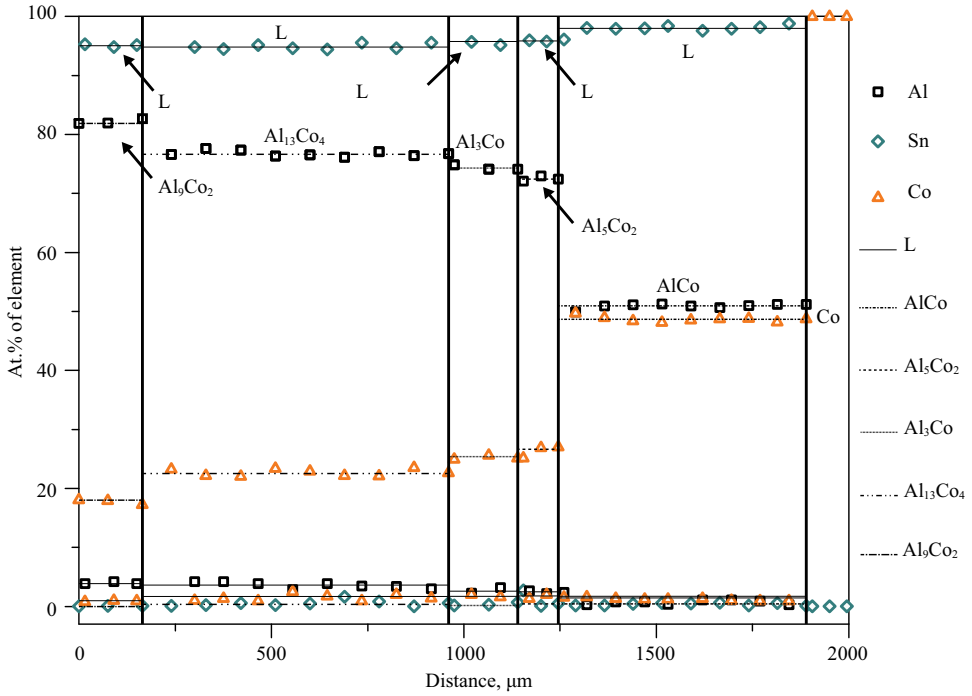

Fig. 8 Composition profile of diffusion couple 1 along the line scan shown in Fig. 7

proper time so that all liquid has diffused into the solid. But when the annealing time is proper, every diffusion layer could be treated as local two-phase equilibrium. In this study, each layer was considered to be local two-phase equilibrium. The WDS line scans were used to determine solubility ranges and phase equilibria. For liquid phase, surface analysis by EDS along the line scan was used to determine the solubility ranges. As shown in Fig. 8, the composition profile of diffusion couple 1 was described according to the data that have good consistency in line scan. The same approach was also used to study diffusion couple 2. Figure 7(a) is the microstructure of diffusion couple 1. There are five diffusion layers in diffusion couple 1. Diffusion layers containing three phases are impossible in a ternary system. The reason follows directly from the phase rule. In binary system, three degrees of freedom are required to fix temperature and pressure and vary the composition. Reaction morphologies consisting of two-phase structures are, therefore, thermodynamically forbidden for binary system, assuming that only volume-diffusion take place. In ternary system, it is possible to develop two-phase areas in the diffusion zone because of the extra degree of freedom. That is also the reason why it is impossible to develop three-phase areas.[33] The sequence of phases along the diffusion path can be deduced as: AlCo + L, Al_5Co_2 + L, Al_3Co + L, $Al_{13}Co_4$ + L and Al_9Co_2 + L, which were confirmed by line scan (Fig. 8). According to the analysis, the first diffusion layer is AlCo + L, which is about 740 μm. After that the diffusion path reached Al_5Co_2 + L, Al_3Co + L and $Al_{13}Co_4$ + L, respectively. Because the average atomic numbers of Al_5Co_2, Al_3Co and $Al_{13}Co_4$ are very similar, these layers are not obvious. Figure 7(b, c) are magnifications of these areas. The last diffusion layer is Al_9Co_2 + L. This layer is about 180 μm in width. In diffusion couple 1, the solid solubility of Sn in the Al-Co binary compounds is less than 1 at.%. The phase relationship of Al_3Co + $Al_{13}Co_4$ + L was confirmed by diffusion couple 1.

The diffusion couple 2 was also used to confirm the three-phase region of Al_3Co + $Al_{13}Co_4$ + L at 1000°C. The BSE images in Fig. 9(a)-(c) show the formation of a small region with four diffusion layers. Based on the WDS

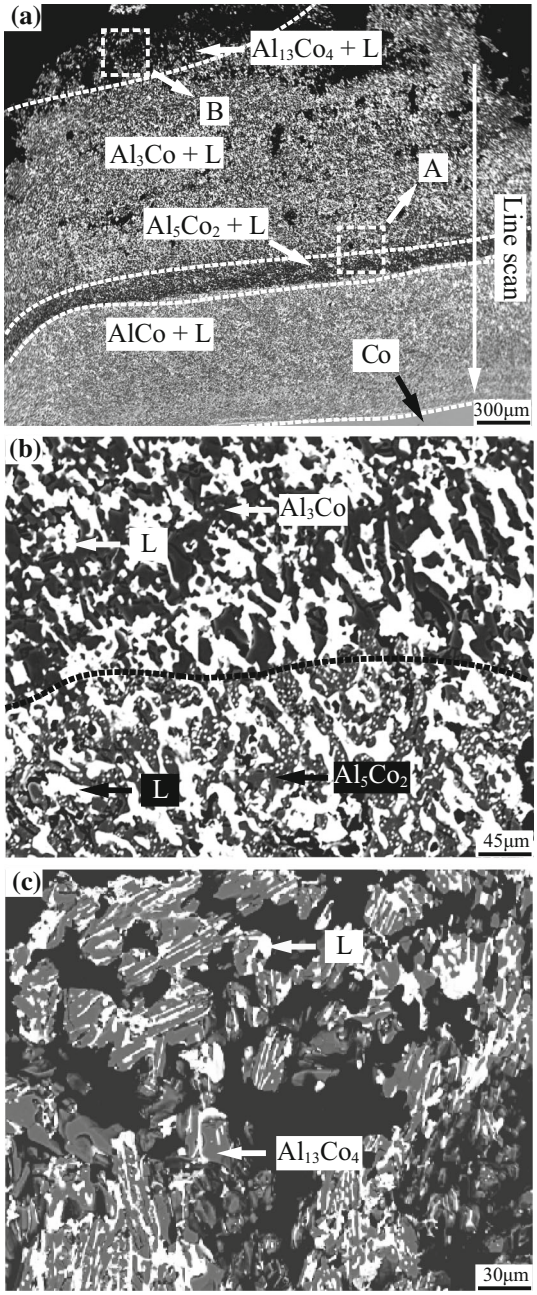

Fig. 9 (a) BSE images of diffusion couple 2; (b) Magnified area of "A" in (a); (c) Magnified area of "B" in (a)

line scan, as shown in Fig. 10, it reveals four two-phase regions. Phase relations confirmed by this diffusion couple are AlCo + L, Al_5Co_2 + L, Al_3Co + L and $Al_{13}Co_4$ + L. This is in agreement with the previous key sample analysis.

3.4 Separated Microscopic Morphology

Furthermore, the as-cast alloy $Al_{47}Sn_{47}Co_6$ had separated macroscopic morphologies, which was caused by liquid miscibility gaps. At a certain temperature, the reaction of Liquid → $Liquid_1$ + $Liquid_2$ occurs. After quenching into ice water, separated microscopic morphology has been retained. Separated macroscopic morphology is shown in Fig. 11(b), where the interlayer is Sn-rich. The insets are microscopic morphologies. This phenomenon is considered to be jointly induced by the degree of subcooling and the density difference of the Al-rich and Sn-rich liquids during cooling under the gravity condition. In addition to these reasons, the magnetic stirrer in the argon arc furnace also has a great influence on this phenomenon. As shown in Fig. 11(a), the alloy $Al_{48}Sn_{48}Co_4$ does not have the separated macroscopic morphology. With the increase of Co content, the macroscopic morphology showed obvious interface between the Sn-rich and Al-rich phases. The Al-rich in macroscopic morphologies is bright, but is dark in microscopic morphologies. Because the color of macroscopic morphologies taken by high resolution camera is based on metallic luster, the color of microscopic morphologies that were measured by EPMA depends on elements' atomic number. The color of the phase will be brighter as the atomic number increases. Same situations were also discovered in alloys $Al_{46}Sn_{46}Co_8$, $Al_{45}Sn_{45}Co_{10}$, $Al_{70}Sn_{10}Co_{20}$, $Al_{64}Sn_{16}Co_{20}$, $Al_{60}Sn_{20}Co_{20}$, $Al_{55}Sn_{25}Co_{20}$, $Al_{83}Sn_{10}Co_7$, $Al_{78}Sn_{10}Co_{12}$, $Al_{73}Sn_{10}Co_{17}$, $Al_{67}Sn_{10}Co_{23}$ and $Al_{66}Sn_{10}Co_{24}$. This result illustrated that Co can promote the liquid-phase separation.

4 Conclusions

1. The isothermal sections of the Al-Sn-Co system at 800 and 1000 °C for the whole composition range were experimentally determined. A total of seven and five three-phase regions exist in the ternary system at 800 and 1000 °C, respectively. There is no ternary compound in this system.
2. The homogeneity ranges of binary compounds were determined and the phase relations among them were established. The solid solubility of Sn in Al-Co binary compounds is small which is from 0.1 to 1.9 at.% at 800 and 1000 °C.
3. Separated microstructure was found in certain Al-Sn-Co alloys. Furthermore, it was found Co additions to

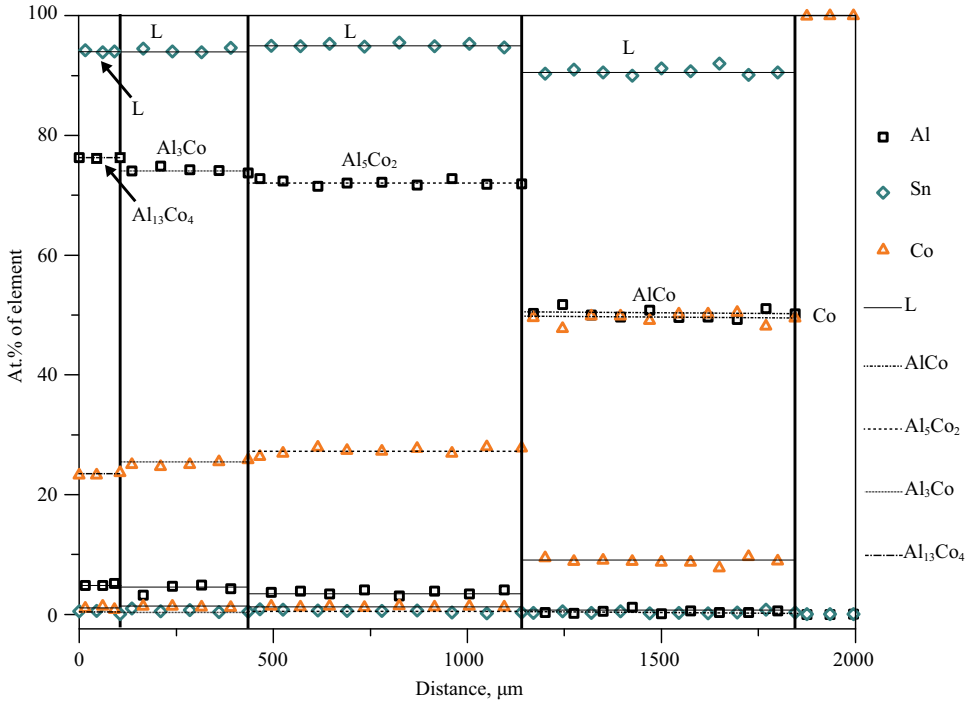

Fig. 10 Composition profile of diffusion couple 2 along the line scan shown in Fig. 9

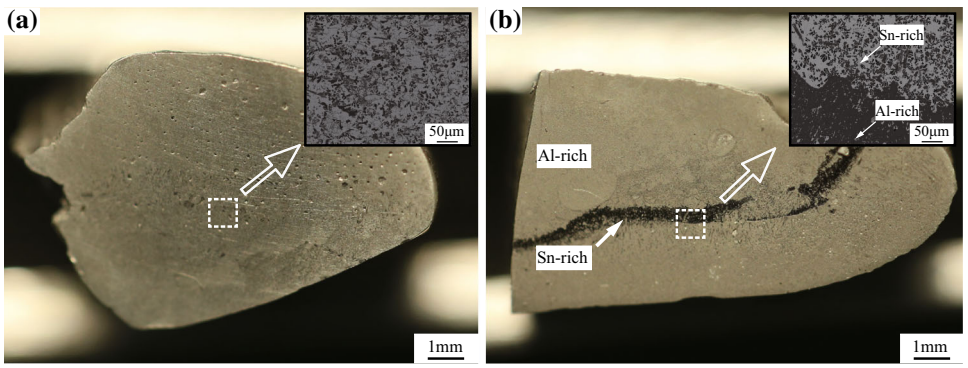

Fig. 11 Macroscopic morphologies of the as-cast alloys (a) $Al_{48}Sn_{48}Co_4$ and (b) $Al_{47}Sn_{47}Co_6$ cooling in the arc-melting furnace, the insets are microscopic morphologies

the Al-Sn binary alloys can effectively promote the liquid phase separation.

Acknowledgments This work was supported by the National Natural Science Foundation of China (Grant No. 51771158).

References

1. H.Z. Wang, D.Y.C. Leung, M.K.H. Leung, and M. Ni, A Review on Hydrogen Production Using Aluminum and Aluminum Alloys, *Renew. Sust. Energy Rev.*, 2009, **13**(4), p 845–853
2. A. Bauen, Future Energy Sources and Systems-Acting on Climate Change and Energy Security, *J. Power Sources*, 2006, **157**(2), p 893–901
3. L. Soler, J. Macanás, M. Muñoz, and J. Casado, Electrocatalytic Production of Hydrogen Boosted by Organic Pollutants and Visible Light, *Int. J. Hydrogen Energy*, 2006, **31**(1), p 129–139
4. M.Q. Fan, F. Xu, and L.X. Sun, Studies on Hydrogen Generation Characteristics of Hydrolysis of the Ball Milling Al-Based Materials in Pure Water, *Int. J. Hydrogen Energy*, 2007, **32**(14), p 2809–2815
5. H. Wang, Y. Chang, S. Dong, Z. Lei, Q. Zhu, P. Luo, and Z. Xie, Investigation on Hydrogen Production Using Multicomponent Aluminum Alloys at Mild Conditions and Its Mechanism, *Int. J. Hydrogen Energy*, 2013, **38**(3), p 1236–1243
6. A.V. Ilyukhina, O.V. Kravchenko, B.M. Bulychev, and E.I. Shkolnikov, Mechanochemical activation of aluminum with gallams for hydrogen evolution from water, *Int. J. Hydrogen Energy*, 2010, **35**(5), p 1905–1910
7. X. Chen, Z. Zhao, M. Hao, and D. Wang, Hydrogen Generation by Splitting Water with Al-Li Alloys, *Int. J. Energy Res.*, 2013, **37**(13), p 1624–1634
8. Z. Zhao, X. Chen, and M. Hao, Hydrogen Generation by Splitting Water with Al-Ca Alloy, *Energy*, 2011, **36**(5), p 2782–2787
9. H. Luo, J. Liu, X. Pu, J. Liang, Z. Wang, F. Wang, K. Zhang, Y. Peng, B. Xu, and J. Li, Hydrogen Generation from Highly Activated Al-Ce Composite Materials in Pure Water, *J. Am. Ceram. Soc.*, 2011, **94**(11), p 3976–3982
10. C.P. Wang, X.J. Liu, I. Ohnuma, R. Kainuma, and K. Ishida, Formation of Immiscible Alloy Powders with Egg-Type Microstructure, *Science*, 2002, **297**(5583), p 990–993

11. C. Wang, Y. Liu, H. Liu, T. Yang, X. Chen, S. Yang and X. Liu, A Novel Self-Assembling Al-based Composite Powder with High Hydrogen Generation Efficiency, *Sci. Rep.-UK*, 2015, **5**, p 17428
12. Y. Liu, X. Liu, X. Chen, S. Yang, and C. Wang, Hydrogen Generation from Hydrolysis of Activated Al-Bi, Al-Sn Powders Prepared by Gas Atomization Method, *Int. J. Hydrogen Energy*, 2017, **42**(16), p 10943–10951
13. X.J. Liu, Y. Liu, Y.H. Guo, D. Wang, S.Y. Yang, Y. Lu, and C.P. Wang, Experimental Investigation and Thermodynamic Calculation of the Phase Equilibria in the Cu-Nb-Zr Ternary System, *J. Phase Equilib. Diffus.*, 2016, **37**(5), p 513–523
14. Y. Yu, X. Liu, Z. Jiang, C. Wang, R. Kainuma, and K. Ishida, Thermodynamics and Liquid Phase Separation in the Cu-Co-Nb Ternary Alloys, *J. Mater. Res.*, 2010, **25**(9), p 1706–1717
15. H.X. Liu, C.P. Wang, Y. Yu, X.J. Liu, Y. Takaku, I. Ohnuma, R. Kainuma, and K. Ishida, Experimental Investigation and Thermodynamic Calculation of the Phase Equilibria in the Al-Bi-Sn Ternary System, *J. Phase Equilib. Diffus.*, 2012, **33**(1), p 9–19
16. J. Liang, L.J. Gao, N.N. Miao, Y.J. Chai, N. Wang, and X.Q. Song, Hydrogen Generation by Reaction of Al-M (M = Fe Co, Ni) with Water, *Energy*, 2016, **113**, p 282–287
17. E.A. Abou-Saif, M. Abd-Rabo, M.M. Ezzo, A.A. Gamil, and A.A. Mohamed, Effect of Heat Treatment on the Structure and Mechanical Properties of Aluminium-Tin Alloys, *Phys. Status Solidi B*, 2010, **67**(2), p K101–K105
18. M. Wolcyrz, R. Kubiak, and S. Maciejewski, X-ray Investigation of Thermal Expansion and Atomic Thermal Vibrations of Tin, Indium, and Their Alloys, *Phys. Status Solidi B*, 2010, **107**(1), p 245–253
19. A.K. Chakrabarty and K.T. Jacob, Experimental Study of Phase Equilibria in the System Cu-Al-Sn, *J. Phase Equilib. Diffus.*, 2013, **34**(4), p 267–276
20. D.F. Soares, M. Abreu, D. Barros, and F. Castro, Experimental Study of the Cu-Al-Sn Phase Equilibria, Close to the Copper Zone, *J. Min. Metall. B*, 2017, **53**, p 34
21. I. Ansara, J.P. Bros, and M. Gambino, Thermodynamic Analysis of the Germanium-Based Ternary Systems (Al-Ga-Ge, Al-Ge-Sn, Ga-Ge-Sn), *CALPHAD*, 1979, **3**(3), p 225–233
22. C.H.F. Stein and N. Dupin, Melting Behaviour and Homogeneity Range of B2 CoAl and Updated Thermodynamic Description of the Al-Co System, *Intermetallics*, 2013, **39**(8), p 58–68
23. Y. Wang and G. Cacciamani, Experimental Investigation and Thermodynamic Assessment of the Al-Co-Ni System, *CALPHAD*, 2018, **61**, p 198–210
24. P. Wang, W. Xiong, U.R. Kattner, C.E. Campbell, E.A. Lass, O.Y. Kontsevoi, and G.B. Olson, Thermodynamic Re-assessment of the Al-Co-W System, *CALPHAD*, 2017, **59**, p 112–130
25. B. Grushko, G. Cacciamani, M. Materials Science International Team, Al-Co Binary Phase Diagram Evaluation Phase diagrams, crystallographic and thermodynamic data: Datasheet from MSI Eureka in SpringerMaterials, *MSI Materials Science International Services GmbH*
26. L. Liu, C. Andersson, and J. Liu, Thermodynamic Assessment of the Sn-Co Lead-Free Solder System, *J. Electron. Mater.*, 2004, **33**(9), p 935–939
27. M. Jiang, J. Sato, I. Ohnuma, R. Kainuma, and K. Ishida, A Thermodynamic Assessment of the Co-Sn System, *CALPHAD*, 2004, **28**(2), p 213–220
28. M. Bulanova, N. Kolchugina, Zienert, T. Nadine Heiden, M. Materials Science International Team, Co-Sn Binary Phase Diagram Evaluation Phase diagrams, crystallographic and thermodynamic data: Datasheet from MSI Eureka in SpringerMaterials, *MSI Materials Science International Services GmbH*
29. J.C. Zhao, A Combinatorial Approach for Efficient Mapping of Phase Diagrams and Properties, *J. Mater. Res.*, 2001, **16**(6), p 1565–1578
30. F.J.J.V. Loo, Multiphase Diffusion in Binary and Ternary Solid-State Systems, *Prog. Solid State Ch.*, 1990, **20**(1), p 47–99
31. A.A. Kodentsov, G.F. Bastin, and F.J.J.V. Loo, The Diffusion Couple Technique in Phase Diagram Determination, *J. Alloys Compd.*, 2001, **320**(2), p 207–217
32. J.C. Zhao, M.R. Jackson, and L.A. Peluso, Determination of the Nb-Cr-Si Phase Diagram Using Diffusion Multiples, *Acta Mater.*, 2003, **51**(20), p 6395–6405
33. J.C. Zhao, Application of diffusion couples in phase diagram determination, *Methods for phase diagram determination*, 1st ed, Elsevier, 2011, p 223–224